Crystal Structures, Dimorphism and Lithium Mobility of Li_7MO_6 (M = Bi, Ru, Os)

Claus Mühle, Andrey Karpov, Aswin Verhoeven, and Martin Jansen*

Stuttgart, Germany, Max-Planck-Institut für Festkörperforschung

Received March 6th, 2005.

Abstract. Li_7MO_6 (M = Bi, Ru, Os) have been synthesized by solid state reaction of Li_2O with Bi_2O_3, or MO_2 (M = Ru, Os) and characterized using powder X-ray diffraction, differential scanning calorimetry, magnetic susceptibility (for M = Ru, Os), ionic conductivity and ^{6}Li solid state NMR (for M = Bi) measurements. All three compounds exhibit a temperature induced triclinic − rhombohedral phase transition. Structures of the new low temperature triclinic phases have been refined by the Rietveld method from powder X-ray data using atomic parameters of Li_7TaO_6 as a starting model (**Li_7BiO_6**: triclinic, $P\bar{1}$, a = 5.5071(1), b = 6.0425(1), c = 5.5231(1) Å, α = 116.912(1), β = 120.867(1), γ = 62.234(1)°, V = 133.96(1) Å^3, Z = 1, T = 230 K; **Li_7RuO_6**: triclinic, $P\bar{1}$, a = 5.3654(1), b = 5.8584(1), c = 5.3496(1) Å, α = 117.182(1), β = 119.117(1), γ = 62.632(1)°, V = 124.43(1) Å^3, Z = 1, T = 295 K; **Li_7OsO_6**: triclinic, $P\bar{1}$, a = 5.3786(1), b = 5.8725(1), c = 5.3591(1) Å, α = 117.193(1), β = 119.277(1), γ = 62.700(1)°, V = 125.15(1) Å^3, Z = 1, T = 295 K). Upon cooling, Li_7RuO_6 and Li_7OsO_6 undergo a magnetic transition at 12 and 13 K, respectively, from the paramagnetic to the antiferromagnetic state. The higher ionic conductivity of Li_7BiO_6 at T < 300 °C, as compared to Li_7RuO_6 and Li_7OsO_6, can be ascribed to the undergoing of the triclinic − rhombohedral transition at a much lower temperature. At T > 300 °C, the ionic conductivity of all three compounds increases sharply due to the melting of the lithium sublattice; for Li_7RuO_6 and Li_7OsO_6 the latter effect is superimposed by the phase transitions to the rhombohedral modifications.

Keywords: Crystal structure; Ionic conductivity; Lithiumhexaoxometallate; Rietveld refinement; X-ray powder diffraction

Introduction

There exists an extended family of lithium hexaoxometallates that show quite similar structural characteristics, despite of their different general compositions Li_6MO_6, Li_7MO_6 and Li_8MO_6. Basic features are triple slabs of composition $[Li_2MO_6]$ with the cations occupying the octahedral voids of two close packed oxygen layers. These slabs are stacked in a way that an approximate hexagonal close packing of oxygen atoms results. Depending on the formula type, the tetrahedral interstices resulting between each two slabs $[Li_2MO_6]$ are fully (Li_8MO_6), or partly (Li_7MO_6 and Li_6MO_6), occupied. This class of compounds has attracted renewed attention since the defective character of the lithium partial structures offers promising prospects with respect to ionic conductivity and might lay a basis for intercalation and deintercalation experiments. A comprehensive compilation of all representatives is given at [1]. More recent works [2, 3] are focusing on lithium ionic conductivity. To all representatives of formula types Li_7MO_6 and Li_8MO_6 trigonal symmetry with space groups $R3$, or $R\bar{3}$ was assigned, previously. However, during our reinvestigation on Li_7MO_6 (M = Nb, Ta, Sb) [4] we noticed slight splittings of powder X-ray diffraction peaks, reducing the symmetry to triclinic ($P\bar{1}$).

* Prof. Dr. M. Jansen
Max-Planck-Institut für Festkörperforschung
Heisenbergstr. 1, D-70569, Germany
Fax: +49-(0)711-689-1502
E-mail: M.Jansen@fkf.mpg.de

Here we report on three further examples of the triclinic − rhombohedral dimorphism in lithiumhexaoxometallates, observed for Li_7BiO_6, Li_7RuO_6 and Li_7OsO_6. The temperatures of the phase transitions have been determined using differential scanning calorimetry (DSC) and temperature dependent X-ray diffractometry. The structures of the low temperature triclinic modifications have been refined by the Rietveld method from laboratory X-ray diffraction data. Li mobility has been studied by impedance and ^{6}Li solid state nuclear magnetic resonance (NMR) spectroscopy.

Results and Discussion

Syntheses

Starting from binary components, Li_7BiO_6 and Li_7RuO_6 have been synthesized through solid state reaction in a flow of oxygen. For Li_7RuO_6 [5] an excess of LiOH has been used. Nevertheless we got always obtained samples containing small amounts of Li_3RuO_4 [6] and of a second, unknown phase [7] together with some Li_2O. Attempts to synthesize Li_7OsO_6 at the same conditions as Li_7BiO_6 and Li_7RuO_6 led to oxidation of osmium to +7 with the formation of known Li_5OsO_6 [8]. In order to stabilize osmium in a lower oxidation state, OsO_2 and Li_2O have been allowed to react under Ar in a closed capsule giving Li_7OsO_6, small quantities of Li_2O and metallic Os, as admixtures. By repeated grinding and annealing the formation of impurity phases could be reduced, but not fully suppressed. The compounds are colourless (Li_7BiO_6), brown (Li_7RuO_6) and black (Li_7OsO_6). If exposed to air, they slowly absorb car-

 DOI: 10.1002/zaac.200500231

Table 1 Temperatures of the phase transition triclinic − rhombohedral for Li_7MO_6, (M = Bi, Ru, Os).

	X-ray powder diffraction data (3 °C/min)	DSC, onset of peaks (10 °C/min)
Li_7BiO_6	−	7 °C
Li_7RuO_6	460−480 °C	450 °C
Li_7OsO_6	350−370 °C	365 °C

bon dioxide and water which is becoming detectable after a few days by DTA. These compounds evolve oxygen at $T \approx 1000$ °C.

DSC Analysis and Temperature-Dependent X-ray Powder Diffractometry

All three compounds were checked for possible phase transitions by DSC measurements and temperature dependent X-ray diffractometry. By means of DSC, upon cooling, an endothermal effect at $T = 7$ °C was observed for Li_7BiO_6. The corresponding low temperature X-ray diffractogram, recorded at $T = -43$ °C (230 K), allows to connect this peak with a transition of the well known rhombohedral modification of Li_7BiO_6, stable at room temperature [9], to a triclinic one. High temperature X-ray powder diffraction patterns of triclinic Li_7RuO_6 and Li_7OsO_6 show a phase transition to the rhombohedral form in a range of T = 460 − 480 °C and T = 350 − 370 °C, correspondingly. The associated peaks in the DSC are observed at T = 450 °C and T = 365 °C (see Table 1). Hence, all three lithiumoxometalates obtained follow to the same transition scheme from triclinic (LT) to rhomohedral (HT) as reported previously for Li_7MO_6 (M = Nb, Ta, Sb) [4].

Crystal Structures of Triclinic Modifications of Li_7MO_6 (M = Bi, Ru, Os)

Using high resolution synchrotron powder data, we have determined and refined the crystal structure of Li_7TaO_6 at room temperature by Fourier techniques and Rietveld refinement, respectively [4]. This first example of a triclinic modification of the lithium-rich hexaoxometallates was refined assuming equal partial occupations for all four different lithium positions. Following this model we have refined the new structures by the Rietveld method from powder XRD patterns in the space group $P\bar{1}$, fixing the occupation factors of lithium atoms at 0.875. The details of the refinement and structural parameters are listed in Tables 2 and 3. The refinement has led to a good coincidence of the calculated intensities to the measured XRD patterns (Fig. 1−3).

The characteristic feature of the structure is a slightly distorted hexagonal closed packing of oxygen atoms (Fig. 4). The heavy metal atoms Bi, Ru and Os are placed at the origin of the unit cell and surrounded by six oxygen atoms in shape of virtually ideal octahedra (Table 4). The averaged M−O distances ($\bar{d}$(Bi−O) = 2.145 Å, $\bar{d}$(Ru−O) = 1.980 Å, $\bar{d}$(Os−O) = 1.998 Å) agree well with distances found in analogous compounds of pentavalent metals in octahedral coordination, or with the sum of crystal radii reported for oxides for coordination numbers CN = VI [10] ($\bar{d}(Bi^{5+}-O)$ = 2.13 Å for Na_3BiO_4 [11], or 2.16 Å [10], $\bar{d}(Ru^{5+}-O)$ = 1.986 Å in Sr_3LiRuO_6 [12] or 1.965 Å [10], $\bar{d}(Os^{5+}-O)$ = 1.97 Å [10]). The O−M−O angles diverge but insignificantly from 90°. The MO_6 octahedra are connected to each other via strongly distorted octahedra of $Li(4)O_6$. Half of the tetrahedral interstices between resulting slabs [Li(4)MO2] are filled with Li1−Li3 atoms building a double layer of edge-shared ($Li(1-3)O_4$) tetra-

Table 2 Crystallographic data and details on refinement for triclinic modifications of Li_7MO_6, M = (Bi, Ru, Os).

	Li_7BiO_6	Li_7RuO_6	Li_7OsO_6
space group	$P\bar{1}$	$P\bar{1}$	$P\bar{1}$
a /Å	5.5071(1)	5.3654(1)	5.3786(1)
b /Å	6.0425(1)	5.8584(1)	5.8725(1)
c /Å	5.5231(1)	5.3496(1)	5.3591(1)
α /°	116.912(1)	117.182(1)	117.193(1)
β /°	120.867(1)	119.117(1)	119.277(1)
γ /°	62.234(1)	62.632(1)	62.700(1)
V /Å^3	133.96(1)	124.43(1)	125.15(1)
Z	1	1	1
T /K	230	295	295
formula weight /g·mol^{-1}	353.56	245.65	334.78
ρ_{calc} /g·cm^{-3}	4.383	3.365	4.436
radiation source, monochromator	Cu-$K_{\alpha1}$, germanium	Cu-$K_{\alpha1}$, germanium	Cu-$K_{\alpha1}$, germanium
cappilary diameter	0.3	0.3	0.3
2 Θ range, step width /°	12 to 105, 0.01	5 to 105, 0.01	5 to 110, 0.01
No. of refined parameters	39	39	39
R_p /% [a]	6.35	5.44	5.21
R_{wp} /% [a]	8.23	7.45	6.92
R_F /% [a]	2.47	3.92	2.39
χ^2 [a]	1.92	1.39	1.61

[a] R_p, R_{wp}, R_F and ^{2} as defined in FullProf

hedra. The eight lithium positions within the unit cell build a distorted cube with a mean Li−Li distance of 2.39(5) Å for Li_7BiO_6, 2.41(3) Å for Li_7RuO_6 and 2.40(4) Å for Li_7OsO_6 (Table 3, Fig. 5), excellently agreeing with the value found for Li_7TaO_6 (2.41 Å) [4].

Magnetic Properties

Magnetization of the samples has been measured at three different magnetic fields of 1, 3 and 5 T. A small field dependence of the samples susceptibilities has been corrected by extrapolation of the measured values to $1/H \rightarrow 0$. Fig. 6 and 7 (squares) show the temperature dependencies of the magnetic susceptibilities for Li_7RuO_6 and Li_7OsO_6 after correction for the weights of the samples due to small quantities of diamagnetic impurities of Li_2O and others and, finally, for the core diamagnetism ($-113 \cdot 10^{-11}$ $m^3 \cdot mol^{-1}$ for Li_7RuO_6 and $-125 \cdot 10^{-11}$ $m^3 \cdot mol^{-1}$ for Li_7OsO_6 [13], p. 426). Upon cooling the compounds undergo a transition

Table 3 Atomic parameters and isotropic thermal displacement parameters for triclinic modifications of Li_7MO_6, M = (Bi, Ru, Os).

Atom	occupancy	*x*	*y*	*z*	B_{eq} /Å^2
Bi					1.43(1)
Ru	1	0	0	0	1.51(1)
Os					1.57(1)
		0.911(2)	0.244(1)	0.393(2)	2.41(8)
O1	1	0.8996(9)	0.2362(9)	0.3695(8)	2.00(6)
		0.912(1)	0.235(1)	0.379(1)	2.13(8)
		0.253(1)	0.237(1)	0.085(2)	2.41(8)
O2	1	0.225(1)	0.2311(9)	0.081(1)	2.00(6)
		0.217(2)	0.243(2)	0.081(2)	2.13(8)
		0.386(1)	0.751(1)	0.230(2)	2.41(8)
O3	1	0.3700(9)	0.7835(8)	0.2372(9)	2.00(6)
		0.374(1)	0.780(1)	0.232(1)	2.13(8)
		0.489(5)	0.368(4)	0.070(6)	3.1(2)
Li1	0.875	0.498(3)	0.378(3)	0.105(3)	3.9(2)
		0.501(5)	0.399(5)	0.097(5)	2.9(2)
		0.123(5)	0.622(5)	0.190(5)	3.1(2)
Li2	0.875	0.101(3)	0.649(4)	0.219(3)	3.9(2)
		0.109(5)	0.686(5)	0.252(6)	2.9(2)
		0.742(5)	0.635(5)	0.536(5)	3.1(2)
Li3	0.875	0.782(3)	0.655(3)	0.528(3)	3.9(2)
		0.764(5)	0.642(5)	0.501(4)	2.9(2)
		0.657(5)	0.032(4)	0.359(5)	3.1(2)
Li4	0.875	0.637(4)	0.013(2)	0.312(4)	3.9(2)
		0.651(5)	0.019(3)	0.315(6)	2.9(2)

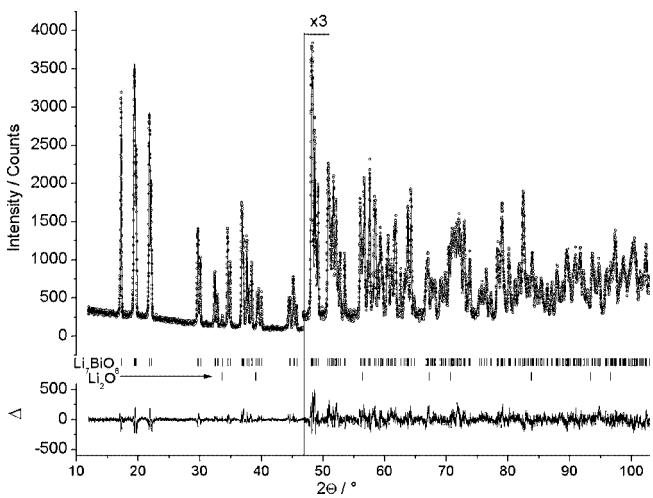

Fig. 1 Observed and calculated powder X-ray diffraction patterns for Li_7BiO_6 at 230 K. Shown are the observed (circles) and calculated (solid line) data and the enlarged difference curve between observed and calculated profiles (below in an additional window). Vertical lines indicate the Bragg reflection positions for Li_7BiO_6 (top) and Li_2O (bottom). The high angle part is enlarged for clarity.

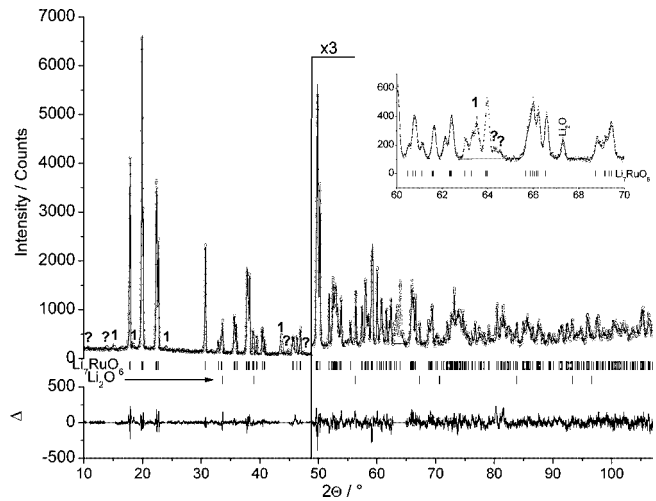

Fig. 2 Observed and calculated powder X-ray diffraction patterns for Li_7RuO_6 at room temperature. Shown are the observed (circles) and calculated (solid line) data and the enlarged difference curve between observed and calculated profiles (below in an additional window). Vertical lines indicate the Bragg reflection positions for Li_7RuO_6 (top) and Li_2O (bottom). Peaks of the Li_3RuO_4 admixture are indicated by "1" and of an unknown phase by "?". The high angle part is enlarged for clarity. The excluded region at 2θ from 62.8 to 64.9 degrees is shown in an enlarged scale.

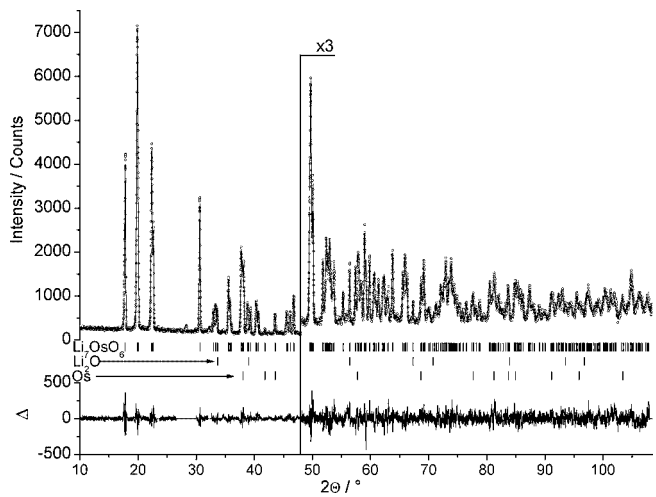

Fig. 3 Observed and calculated powder X-ray diffraction patterns for Li_7OsO_6 at room temperature. Shown are the observed (circles) and calculated (solid line) data and the enlarged difference curve between observed and calculated profiles (below in an additional window). Vertical lines indicate the Bragg reflection positions for Li_7OsO_6 (top) and Li_2O (middle) and Os (bottom). The high angle part is enlarged for clarity.

from the paramagnetic to the antiferromagnetic state at very close Néel temperatures T_N of 12 K for Li_7RuO_6, and 13 K for Li_7OsO_6. These temperatures are similar to other known compounds containing isolated RuO_6^{7-} or OsO_6^{7-} octahedra (T_N = 18 K in La_3RuO_7 [14], T_N = 14 K in $La_7Ru_3O_{18}$ [15], or T_N = 17 K in La_2NaOsO_6 [16]).

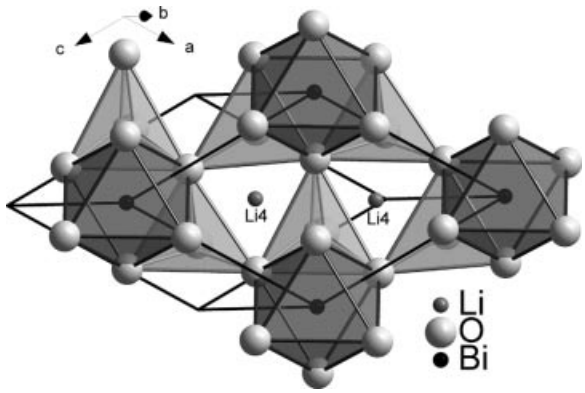

Fig. 4 A schematic representation of the crystal structure of the LT modification of Li_7BiO_6. *In front*: dark-grey BiO_6 octahedra and Li4 atoms building monolayer of $[Li(4)_{1.75}BiO_2]$. *In background*: one layer of light-grey $Li(1-3)O_4$ tetrahedra. Big light-grey spheres exhibiting oxygen atoms build a slightly distorted *hcp* packing.

Table 4 Distances and angles for triclinic modifications Li_7MO_6, M = (Bi, Ru, Os).

distances /Å angles /°	Li_7BiO_6	Li_7RuO_6	Li_7OsO_6
M−O(1)	2.155(8) x 2	1.991(4) x 2	2.008(6) x 2
M−O(2)		1.984(6) x 2	2.011(9) x 2
M−O(3)	2.19(1) x 2 2.093(7) x 2	1.966(5) x 2	1.975(7) x 2
O−M−O	88.4(3) − 91.6(3) 180.0(3)	89.1(3) − 90.9(4) 180.0(4)	89.0(6) − 91.0(6) 180.0(6)
Li(1)−O(1)	2.11(2)	1.95(2)	2.05(3)
Li(1)−O(2)	1.86(4)	1.94(2)	2.07(3)
Li(1)−O(3)	1.83(4)	1.95(2)	1.86(3)
Li(1)−O(3)	1.97(2)	2.01(2)	1.90(3)
O−Li(1)−O	97(1) − 126(2)	92(1) − 116(1)	93(1) − 120(1)
Li(2)−O(1)	2.15(3)	1.99(2)	1.86(3)
Li(2)−O(2)	1.90(2)	1.81(2)	1.84(3)
Li(2)−O(2)	1.98(3)	2.08(2)	2.21(3)
Li(2)−O(3)	1.82(4)	1.88(2)	1.81(3)
O−Li(2)−O	105(1) − 113(1)	99(1) − 122(1)	97(1) − 127(1)
Li(3)−O(1)	2.02(3)	1.84(2)	1.90(3)
Li(3)−O(1)	2.15(4)	2.08(2)	2.03(3)
Li(3)−O(2)	1.86(3)	1.90(2)	1.98(2)
Li(3)−O(3)	1.89(2)	2.02(2)	1.92(3)
O−Li(3)−O	100(1) − 119(1)	98(1) − 124(1)	94(1) − 122(1)
Li(4)−O(1)	2.19(4)	2.17(2)	2.11(3)
Li(4)−O(1)	2.32(2)	2.45(2)	2.39(2)
Li(4)−O(2)	2.11(2)	2.06(2)	2.14(2)
Li(4)−O(2)	2.41(3)	2.20(2)	2.21(3)
Li(4)−O(3)	2.12(3)	2.15(2)	2.20(3)
Li(4)−O(3)	2.41(3)	2.17(2)	2.26(2)
O−Li(4)−O	83(1) − 100(1) 169(1) − 175(1)	74(1) − 100(1) 164(1) − 178(1)	76(1) − 99(1) 166(1) − 178(1)
Li(1)−Li(2)	2.10(4)	2.16(3)	2.27(4)
Li(1)−Li(3)	2.41(3)	2.37(2)	2.18(3)
Li(1)−Li(4)	2.68(5)	2.51(2)	2.61(3)
Li(2)−Li(3)	2.27(5)	2.39(3)	2.49(4)
Li(2)−Li(4)	2.57(3)	2.61(2)	2.34(4)
Li(3)−Li(4)	2.31(3)	2.43(3)	2.49(4)
Li−Li−Li	75(1) − 102(1)	78(1) − 100(1)	78(2) − 97(2)

The high temperature paramagnetic regions of the magnetic curves (60 − 330 K) have been fitted with the program CONDON [17], accounting for the interelectronic repulsion (Racah-Parameters *B* and *C*), ligand-field splitting, spin-orbit coupling (spin-orbit coupling constant ζ), and cooperative interactions in the molecular field approximation. The program is based on the quantum-chemical equations taken from the works of *Condon* and *Shortley* [18], and *Griffith* [19] and has been already successfully applied to the discussion of the magnetic properties of such 5d ions like Re^{3+} [20], Os^{4+} [21], or Os^{6+} [22]. The values of spin-orbit coupling constants for Ru^{5+} (ζ = 1500 cm^{-1}) and Os^{5+} (ζ = 4500 cm^{-1}) have been taken from [23]. The Racah-parameters B = 693 cm^{-1} and C = 2952 cm^{-1} for Os^{5+} have been taken from [13], p. 253. Exact values of Racah-parameters

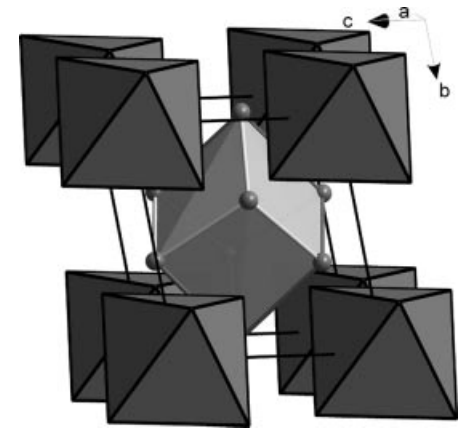

Fig. 5 Perspective view of the crystal structure of the LT modification of Li_7BiO_6. The regular BiO_6-octahedra and the lithium metal positions marking the corners of a distorted cube (lithium sublattice) are drawn.

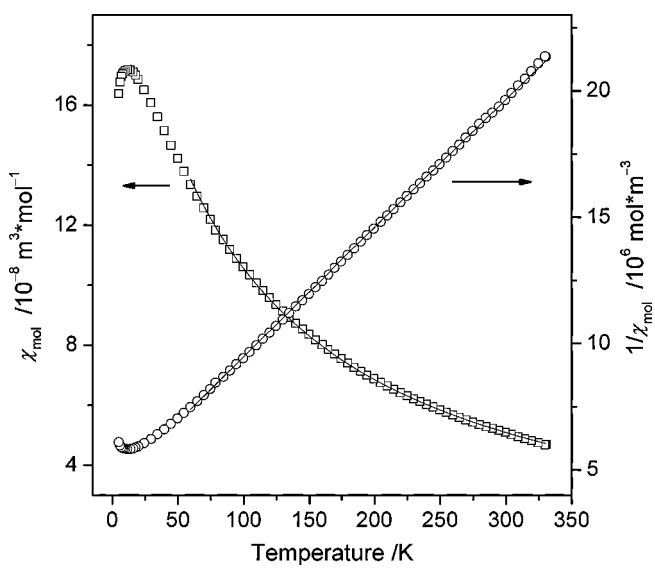

Fig. 6 Temperature dependence of magnetic susceptibility (open squares) and inverse magnetic susceptibility (open circles) of Li_7RuO_6 extrapolated to $1/H \rightarrow 0$. The solid line shows a fit using parameters as described in the text.

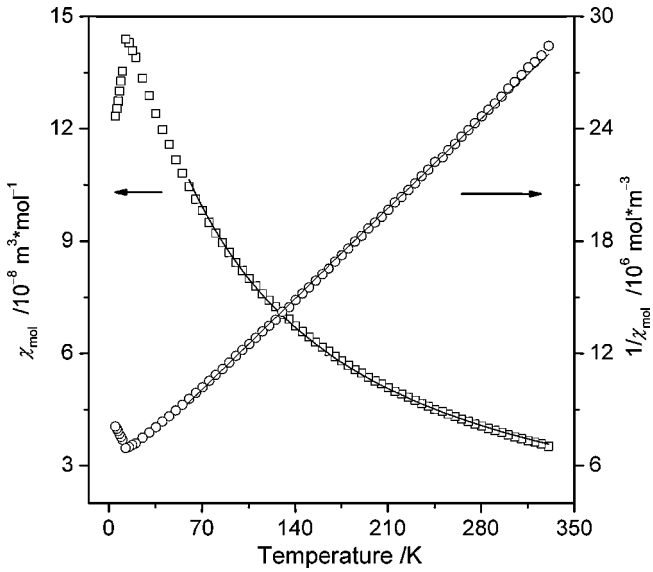

Fig. 7 Temperature dependence of magnetic susceptibility (open squares) and inverse magnetic susceptibility (open circles) of Li_7OsO_6 extrapolated to $1/H \rightarrow 0$. The solid line shows a fit using parameters as described in the text.

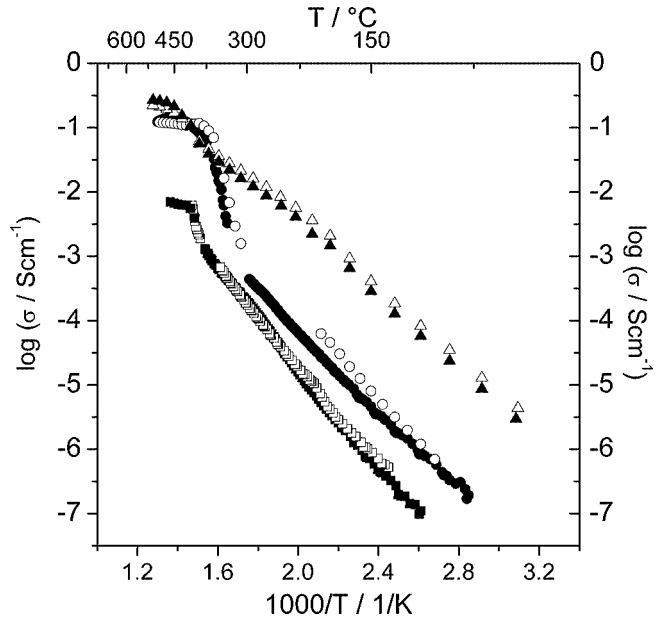

Fig. 8 Temperature dependence of ionic conductivity for Li_7MO_6 (M = Ru (squares), Os (circles), and Bi (triangles). Filled symbols represent heating, open symbols − cooling.

for Ru^{5+} are not known yet, thus they have been obtained by extrapolation of the Racah-parameters for Ru^{3+} (B = 464 cm^{-1}, C = 1875 cm^{-1} [13], p. 252) using common trends of their change with an increasing charge of an ion (B = 500 cm^{-1}, C = 2000 cm^{-1}). For both compounds two parameters have been refined − the ligand-field parameter B_0^4, and the molecular field parameter λ_{MF}. The refinements converged at B_0^4 = 51185 cm^{-1}, $B_4^4 = \sqrt{5/14}\ B_0^4$, $\lambda_{MF} = -4.30\times10^6$ mol·m^{-3} for Li_7RuO_6, and B_0^4 = 84960 cm^{-1}, $B_4^4 = \sqrt{5/14}\ B_0^4$, $\lambda_{MF} = -5.17\times10^6$ mol·m^{-3} for Li_7OsO_6. The calculated fits agree well with the measured susceptibilities (solid lines in Figs. 6, 7; SQ[1)] = 0.5 % for Li_7RuO_6, SQ = 0.7 % for Li_7OsO_6). The resulted ligand-field parameters $D_q = B_0^4$ /21 for cubic symmetry (2437 cm^{-1} for Li_7RuO_6, and 4046 cm^{-1} for Li_7OsO_6) are in the expected region (compare with D_q = 2510 cm^{-1} for 4d^3 Mo^{3+}, D_q = 2860 cm^{-1} for 4d^5 Ru^{3+}, and D_q = 3710 cm^{-1} for 5d^3 Os^{5+}, all in the octahedral H_2O-ligand field [13], p. 253).

Ionic Conductivity

The Arrhenius plots of the temperature-dependent ionic conductivity for Li_7MO_6 (M = Bi [4], Ru, Os) are displayed in Fig. 8. The corresponding activation energies (E_a) as derived from the slopes of the conductivity curves using the Arrhenius equation and the conductivities at selected temperatures are listed in Table 5.

When comparing conductivity in the low temperature region (T < 300 °C), the previously measured rhombohedral bismuthate [2, 4] has a by two orders of magnitude higher ionic conductivity. *Nomura* and *Greenblatt* [2] have ascribed this fact to a reduction of the ion jumps energy barrier in bismuthate due to an optimized size of the lithium-oxygen channel for passage of lithium atoms through it. However our analysis of Li−Li interatomic distances does not reveal any significant distinctions for all Li_7MO_6. The higher conductivity of bismuthate seems more probably caused by the transition from the triclinic modification to the rhombohedral at a much lower temperature (7 °C for Li_7BiO_6) as compared to other Li_7MO_6 (see Table 1). This assumption is supported by NMR investigations on Li_7BiO_6 (see below)

Table 5 Ionic Conductivity (σ) and the Activation Energies (E_a) for Li_7MO_6 (M = Bi, Ru, Os).

	σ/S·cm^{-1}	E_a /eV
Li_7BiO_6 [a)]	110 °C: 8.24×10^{-5}	50−200 °C: 0.58
	150 °C: 4.06×10^{-4}	200−400 °C: 0.48
	300 °C: 1.86×10^{-2}	400−700 °C: 0.27
	450 °C: 0.1718	
Li_7RuO_6	110 °C: 1.10×10^{-7}	110−390 °C: 0.81
	150 °C: 7.18×10^{-7}	420−460 °C: 0.19
	300 °C: 2.08×10^{-4}	
	450 °C: 6.69×10^{-3}	
Li_7OsO_6	110 °C: 8.39×10^{-7}	110−300 °C: 0.66
	150 °C: 4.58×10^{-6}	420−490 °C: 0.13
	300 °C: 4.40×10^{-4}	
	450 °C: 0.1155	

[a)] Data taken from [4]

[1)] SQ = $(FQ/n)^{1/2}\cdot100$ %, with FQ = $\sum_{i=1}^{n}$ {[χ_{obs} (i) − χ_{cal} (1)] / χ_{obs} (i)}^{2}

showing a much higher mobility of lithium ions in the rhombohedral phase as compared to the triclinic one.

On heating, at $390 < T < 420$ °C for Li_7RuO_6 and $300 < T < 380$ °C for Li_7OsO_6 the conductivity increases sharply due to the phase transition to the HT modifications, superimposed with the melting of the lithium sublattice. At higher temperatures the conductivity achieves plateaus. The corresponding low activation energies for conduction in this region indicate almost free motion of Li^+ ions through the structure. The conductivity of the HT forms of Li_7RuO_6 and Li_7OsO_6 is several orders of magnitude higher than the values of the room temperature modifications.

^{6}Li NMR

NMR is widely applied to study the dynamics of chemical processes [24]. ^{6}Li solid-state MAS NMR measurements were performed to study the mobility of the lithium ions in Li_7BiO_6. The lithium-6 nucleus has only a very small electrical quadrupole moment and therefore yields sharp lines under fast magic-angle spinning. If the cation hopping rate is in the same order of magnitude as the separation of the peaks in the NMR spectrum one can study the dynamics by varying the temperature and observing the influence of the motion on the NMR spectrum. The NMR spectra of Li_7BiO_6 at different temperatures are given in Fig. 9. At 225 K we see a superposition of multiple non-resolved peaks. Deconvolution was attempted but unsuccessful, possibly because the chemical shift of a lithium cation depends on both its crystallographic position and on the occupancy of the neighbouring lithium cation sites, which leads to a large number of resonances with slightly different chemical shifts. When we raise the temperature, the lithium cations become more mobile and the different resonances reach coalescence at about 282 K. Further heating sharpens the spectrum, indicating that all lithium sites are exchanging.

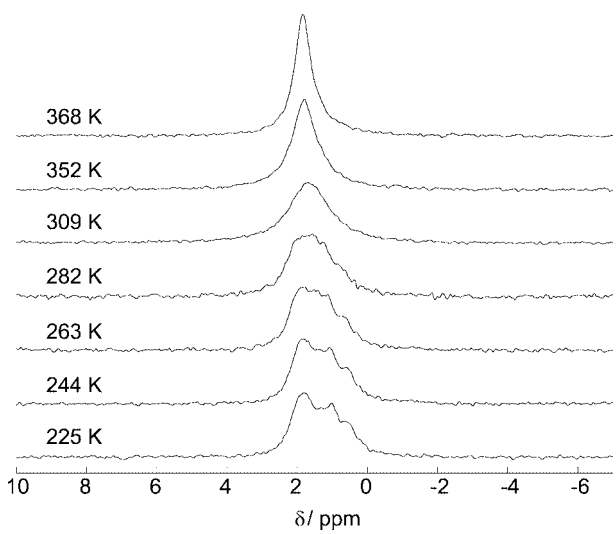

Fig. 9 ^{6}Li MAS NMR spectra of Li_7BiO_6 at different temperatures. $\omega_r/(2\pi) = 14$ kHz.

Experimental Section

Syntheses. The lithium hexaoxometalates have been synthesized by solid-state reaction of mixtures of the respective metal oxides with an excessive amount of lithium hydroxide in a stream of dry oxygen or with a stoichiometric amount of lithium oxide under dry argon. Li_2O was prepared by dehydrating $LiOH{\cdot}H_2O$ (Fluka, 99+ %) in vacuum at $T = 800$ °C [25].

Li_7BiO_6: Mixtures of Bi_2O_3 (Merck, 99.9 %) and $LiOH{\cdot}H_2O$ in a ratio Li/Bi = 7.35 were heated in a nickel boat, placed in a quartz tube, in a flow of dry oxygen at $T = 700$ °C for one day.

Li_7RuO_6: Mixtures of RuO_2 (Alfa-Aesar, 99.95 %) and $LiOH{\cdot}H_2O$ in a ratio Li/Ru = 7.5 were pressed to a pellet and heated in a gold boat, placed in a quartz tube, in a flow of dry oxygen at $T = 950$ °C for two days.

Li_7OsO_6: Mixtures of OsO_2 (Alfa-Aesar, 99.99 %) and Li_2O in a ratio Li/Os = 8.1 were heated in a silver crucible sealed in a quartz ampoule under dry argon atmosphere at $T = 700$ °C for two days.

Characterization. X-ray powder diffraction data of Li_7RuO_6, Li_7OsO_6 at room temperature, and of Li_7BiO_6 at $T = 230$ K, were collected with a Stoe Stadi-P transmission laboratory diffractometer (primary beam Johansson-type Ge-monochromator for Cu-$K_{\alpha1}$-radiation, linear PSD) in steps of 0.01° in 2Θ over different ranges of 2Θ for approximately 24 hours each, with the samples sealed in glass capillaries of 0.3 mm diameter (Hilgenberg, glass No. 50). From visual inspection, it was concluded that Li_7RuO_6, Li_7OsO_6 at room temperature and Li_7BiO_6 at $T = 230$ K are isostructural to triclinic Li_7TaO_6 [4]. The crystal structures of the compounds were refined by the Rietveld method [26] using the FullProf program package [27] and the atomic parameters of Li_7TaO_6 as a starting model. While the lattice constants of Li_7RuO_6 and Li_7OsO_6 differed not very much from those of Li_7TaO_6 and thus were directly refined, for Li_7BiO_6, due to the large difference in volumes, the unit cell was re-indexed by CRYSFIRE [28] using LZON algorithm [29], leading to a successful Rietveld refinement. Small amounts of additional phases (Li_2O in all compounds and Os in the osmonate) noticeable in the XRD patterns were included in the Rietveld refinement with their scale factors, lattice constants, half-widths and peak shapes profile parameters varied. The temperature factors of crystallographically different positions of the same element were constrained.

Temperature dependent Guinier recordings (Enraf-Nonius FR 553, $CuK_{\alpha1}$, Johansson monochromator) were conducted in a temperature range from room temperature to $T = 500$ °C with a heating rate of 3 K/min.

Differential Scanning Calorimetry (DSC) data were recorded on a calorimeter (model 404, Netzsch, Germany) by heating and cooling the sample in an aluminium crucible with 10 K/min from room temperature to $T = 600$ °C.

Magnetization was measured on powder samples of Li_7RuO_6 (57.6 mg) and Li_7OsO_6 (29.2 mg) using a SQUID magnetometer (MPMS-XL7, Quantum Design, USA) in the temperature range 5 − 330 K at fields of 1, 3 and 5 T.

The ionic conductivity was measured using compact polycrystalline powder samples (diameter 6 mm, thicknesses 0.85 mm, pressed with 350 MPa) in an ion-blocking cell Ag/sample/Ag. During the measurement, the samples were placed into a quartz glass cell [30] under dry argon. The temperature dependent ac impedance spectra were measured with a Novocontrol Alpha-A 4.2 Analyzer combined with the impedance interface ZG4 in a 2-wire arrangement

in the frequency range of $\nu = 0.5$ Hz to $\nu = 20$ MHz. Measurements and data recording were performed with the WinDeta program [31]. The bulk conductivity was determined by non linear mean square deviation curve fitting of the impedance spectrum using the WinFit program [32].

All NMR experiments were performed using a Bruker DSX-400 spectrometer operating at 9.4 T with a resonance frequency of 58.8 MHz for ^{6}Li. Chemical shifts were referenced to 1 M aqueous LiCl. The sample was sealed in a Pyrex tube fitting exactly into the MAS rotor. ^{6}Li MAS NMR experiments were performed in the temperature range of 225 K to 368 K using a Bruker 4 mm triple resonance probe at magic-angle spinning frequency of 14 kHz. The temperature was calibrated using the temperature-dependent ^{207}Pb chemical shift of $PbNO_3$ [33].

Acknowledgement. The authors would like to thank *Michael Fischer* and *Ewald Schmitt* for the DSC measurements, *Dr. Christian Oberndorfer* for the DTA, *Denis Orosel* for recording of the temperature dependent X-ray diffraction, *Lars Hildebrandt* for ionic conductivity measurements and *Eva Bruecher* for the magnetic measurements. Special thanks to *Prof. Dr. Welf Bronger* and *Prof. Dr. Helmut Schilder* for the valuable discussions of the magnetic properties and the help with the program CONDON. Financial support by the Fonds der Chemischen Industrie is gratefully acknowledged.

References

[1] J. Hauck, *Z. Naturforsch.* **1969**, *24b*, 1067.
[2] E. Nomura, M. Greenblatt, *J. Solid State Chem.* **1984**, *52*, 91.
[3] E. Nomura, M. Greenblatt, *Solid State Ionics* **1984**, *13*, 249.
[4] C. Mühle, R. E. Dinnebier, L. van Wüllen, G. Schwering, M. Jansen, *Inorg. Chem.* **2004**, *43*, 874.
[5] R. Scholder, H. Gläser, *Z. Anorg. Allg. Chem.* **1964**, *327*, 15.
[6] a) T. S. Bush, C. R. A. Catlow, P. D. Battle, *J. Mater. Chem.* **1995**, *5*, 1269; b) A. Alexander, P. D. Battle, J. C. Burley, D. J. Gallon, C. P. Grey, S. H. Kim, *J. Mater. Chem.* **2003**, *13*, 2612.
[7] I. S. Shaplygin, M. I. Gadzhiev, V. B. Lazarev, *Russ. J. Inorg. Chem.* **1987**, *32*, 418.
[8] T. Betz, R. Hoppe, *Z. Anorg. Allg. Chem.* **1985**, *524*, 17.
[9] R. Scholder, *Angew. Chem.* **1958**, *70*, 583.
[10] R. D. Shannon, *Acta Crystallogr.* **1976**, *A32*, 751.
[11] B. Schwedes, R. Hoppe, *Z. Anorg. Allg. Chem.* **1972**, *393*, 136.
[12] J. Darriet, F. Grasset, P. D. Battle, *Mat. Res. Bull.* **1997**, *32*, 139.
[13] H. Lueken, *Magnetochemie*, Teubner, Stuttgart, Leipzig 1999.
[14] P. Khalifah, D. M. Ho, Q. Huang, R. J. Cava, *J. Solid State Chem.* **2002**, *165*, 359.
[15] P. Khalifah, Q. Huang, D. M. Ho, H. W. Zandbergen, R. J. Cava, *J. Solid State Chem.* **2000**, *155*, 189.
[16] W. R. Gemmill, M. D. Smith, R. Prozorov, H.-C. zur Loye, *Inorg. Chem.* **2005**, *44*, 2639.
[17] H. Schilder, H. Lueken, *J. Magn. Magn. Mater.* **2004**, *281*, 17.
[18] E. U. Condon, G. H. Shortley, *The Theory of Atomic Spectra*, Cambridge University Press 1977.
[19] J. S. Griffith, *The Theory of Transition Metal Ions*, Cambridge University Press 1977.
[20] W. Bronger, G. Auffermann, H. Schilder, *Z. Anorg. Allg. Chem.* **1998**, *624*, 497.
[21] W. Bronger, T. Sommer, G. Auffermann, P. Müller, H. Schilder, *Z. Anorg. Allg. Chem.* **2001**, *627*, 426.
[22] G. Auffermann, W. Bronger, P. Müller, G. Roth, H. Schilder, T. Sommer, *Z. Anorg. Allg. Chem.* **2005**, *631*, 1060.
[23] W. Haberditzl, *Quantenchemie*, Vol. 4, Dr. Alfred Hüthig Verlag, Heidelberg 1979, p. 109.
[24] R. R. Ernst, G. Bodenhausen, A. Wokaun, *Principles of Nuclear Magnetic Resonance in One and Two Dimensions*, Clarendon Press, Oxford 1987.
[25] G. Brauer, *Handbuch der Präparativen Anorganischen Chemie*, 3rd. ed., Vol. 2, F. Enke, Stuttgart 1978, p. 950.
[26] a) H. M. Rietveld, *Acta Crystallogr.* **1967**, *22*, 151; b) H. M. Rietveld, *J. Appl. Crystallogr.* **1969**, *2*, 65.
[27] J. Rodriguez-Carvajal, FULLPROF Version Juli 2001, CEA/Saclay, France, 2001.
[28] R. Shirley, The Crysfire 2002 System for Automatic Powder Indexing: User's Manual, The Lattice Press, 41 Guildford Park Avenue, Guildford, Surrey GU2 7NL, England, 2002.
[29] R. Shirley, D. Louer, *Acta Crystallogr.* **1978**, *A34*, S382.
[30] U. Köhler, *Dissertation*, Univ. Hannover 1987.
[31] Novocontrol GmbH, WinDeta V 4.5, Hundsangen, Germany, 1995–2003.
[32] Novocontrol GmbH, WinFit V 2.9, Hundsangen, Germany, 1996.
[33] A. Bielecki, D. P. Burum, *J. Magn. Reson. A* **1995**, *116*, 215.

